Acta Oceanol. Sin., 2020, Vol. 39, No. 7, P. 1–10
https://doi.org/10.1007/s13131-020-1574-4
http://www.hyxb.org.cn
E-mail: hyxbe@263.net

Impacts of the upper-ocean salinity variations on the decadal sea level change in the Southeast Indian Ocean during the Argo era

Jiamei Huang[1], Wei Zhuang[1, 2*], Xiao-Hai Yan[3, 4], Zelun Wu[1, 4]

[1] State Key Laboratory of Marine Environmental Science, College of Ocean and Earth Sciences, Xiamen University, Xiamen 361102, China

[2] Southern Marine Science and Engineering Guangdong Laboratory (Zhuhai), Zhuhai 519082, China

[3] Joint Center for Ocean Remote Sensing, University of Delaware-Xiamen University, Newark, DE 19716, USA

[4] College of Earth, Ocean, and Environment, University of Delaware, Newark, DE 19716, USA

Received 1 January 2020; accepted 17 February 2020

Abstract

In the past nearly two decades, the Argo Program has created an unprecedented global observing array with continuous *in situ* salinity observations, providing opportunities to extend our knowledge on the variability and effects of ocean salinity. In this study, we utilize the Argo data during 2004–2017, together with the satellite observations and a newly released version of ECCO ocean reanalysis, to explore the decadal salinity variability in the Southeast Indian Ocean (SEIO) and its impacts on the regional sea level changes. Both the observations and ECCO reanalysis show that during the Argo era, sea level in the SEIO and the tropical western Pacific experienced a rapid rise in 2005–2013 and a subsequent decline in 2013–2017. Such a decadal phase reversal in sea level could be explained, to a large extent, by the steric sea level variability in the upper 300 m. Argo data further show that, in the SEIO, both the temperature and salinity changes have significant positive contributions to the decadal sea level variations. This is different from much of the Indo-Pacific region, where the halosteric component often has minor or negative contributions to the regional sea level pattern on decadal timescale. The salinity budget analyses based on the ECCO reanalysis indicate that the decadal salinity change in the upper 300 m of SEIO is mainly caused by the horizontal ocean advection. More detailed decomposition reveals that in the SEIO, there exists a strong meridional salinity front between the tropical low-salinity and subtropical high salinity waters. The meridional component of decadal circulation changes will induce strong cross-front salinity exchange and thus the significant regional salinity variations.

Key words: decadal sea level change, southeast Indian Ocean, halosteric effect, salinity budget

Citation: Huang Jiamei, Zhuang Wei, Yan Xiao-Hai, Wu Zelun. 2020. Impacts of the upper-ocean salinity variations on the decadal sea level change in the Southeast Indian Ocean during the Argo era. Acta Oceanologica Sinica, 39(7): 1–10, doi: 10.1007/s13131-020-1574-4

1 Introduction

As an important consequence of climate variability and change, sea level change has direct impacts on the ecosystem and human life in coastal and island regions. The total sea level variation is the combination of two major effects: the steric and mass-induced (Gill and Niller, 1973). The steric contribution accounts for the expansion and contraction of water column induced by the variations in water temperature or salinity, while the mass-induced contribution reflects changes in the mass of water column due to precipitation/evaporation, melting of land ice, river runoff or the redistribution of water in the ocean. The steric sea level could be further decomposed into thermosteric and halosteric components, corresponding to the effects of temperature and salinity changes, respectively. Previous studies have shown that temperature change is the main contributor to the patterns of regional sea level variability on the seasonal, interannual and decadal timescales (Vinogradov et al., 2008; Stammer et al., 2013; Köhl, 2014; Zhang and Qu, 2015). Nonetheless, the salinity and mass-induced changes could also be important in some specific regions and timescales (Cheng et al., 2013; Wu et al., 2017). For instance, in the subtropical southeast Pacific, the thermosteric and halosteric heights show similar varying magnitudes on decadal timescale (Nidheesh et al., 2013). Overall, the halosteric effect on sea level change has been less investigated than the thermosteric effect owing to the sparseness of historical salinity measurements and the relatively minor contributions from the halosteric sea level. However, with the development of the International Argo (Array for Real-time Geotropic Oceanography) Program, the deployed profiling floats have created the first global array to continuously observe ocean temperature and salinity versus pressure (Roemmich et al., 2009). Argo data record with global coverage has now reached more than fifteen years, thus providing unprecedented *in situ* dataset to study the multiscale salinity variations and their impacts on sea level and circulation changes.

Over the past nearly three decades, global sea level rise has a mean rate of ~3 mm/a (Willis et al., 2010; Chen et al., 2017). However, regional sea level change can deviate substantially

Foundation item: The National Key Research and Development Program of China under contract No. 2019YFA0606702; the SOA Global Change and Air-Sea Interaction Project under contract No. GASI-IPOVAI-01-04; the National Natural Science Foundation of China under contract Nos 41776003, 91858202 and 41630963.
*Corresponding author, E-mail: wzhuang@xmu.edu.cn

from the global mean rate. During the global surface warming slowdown (GSWS) period from the 1990s to the early 2010s, the tropical western Pacific experienced the highest rates of sea level rise in globe, with values exceeding 10 mm/a (Merrifield et al., 2012; Qiu and Chen, 2012). Afterwards, local sea level in the western Pacific abruptly shifts to a negative trend, probably related to the phase change of Interdecadal Pacific Oscillation (IPO, Hamlington et al., 2016). Due to the oceanic connectivity around the Indonesian Archipelago, sea level signals in the low-latitude western Pacific could be partly transmitted into the Indian Ocean in the form of coastally trapped waves, resulting in significant sea level fluctuations in the southeast Indian Ocean (SEIO, Wijffels and Meyers, 2004). Previous studies have noted that due to the existence of these inter-basin waveguides via the Indonesian Seas, sea level signals near the western coast of Australia and in the western Pacific display very similar oscillations and are both strongly influenced by the Pacific climate modes, e.g., El Niño-Southern Oscillation (ENSO) and IPO (Cai et al., 2005; Feng et al., 2010, Du et al., 2019).

The southern Indian Ocean (SIO) has a unique circulation system that is substantially influenced by the Indonesian Throughflow (ITF), the only low-latitude inter-ocean flow in globe (Schott et al., 2009). Existing comprehensive studies have already shown that the surface heat flux and ocean internal variability are the primary causes for the decadal sea level variability in the subtropical SIO, with the ITF making significant contributions mainly in the SEIO (Li and Han, 2015; Han et al., 2018). On the other hand, despite the coherent decadal sea level variations along the Indo-Pacific inter-basin waveguides, the relative contributions from thermosteric and halosteric components are distinct between basins. In both the north and south Pacific, the rapid sea level rises during the GSWS are mainly thermosteric in nature (Qiu and Chen, 2012; Zhang and Qu, 2015). The exceptional situation exists in the SEIO where the thermosteric and halosteric components are both essential for the rise of steric height during the Argo era from 2005 to 2013 (Llove and Lee, 2015). Estimations based on both the Argo data and the ocean reanalysis product further quantified that halosteric component could explain ~40% of the total SIO sea level rise during the GSWS (Jyoti et al., 2019). The halosteric sea level rise is associated with a decadal freshening in the upper 300 m, which could not be explained by local atmosphere forcing, such as Ekman pumping, precipitation, or the transmission of wave signals from the western Pacific (Llove and Lee, 2015). Some studies inferred that the decadal strengthening of ITF during the GSWS may enhance freshwater transport from Pacific into SIO and thus lead to the freshening phenomenon (Du et al., 2015, 2019; Hu and Sprintall, 2017; Jyoti et al., 2019). In addition to the impact on regional sea level change, salinity effect also plays important roles in regulating or indicating the circulation and climate variability in the SIO. For instance, the intensity of Eastern Gyral Current (EGC) has been found to be largely modulated by the salinity front between the fresher tropical water and saltier subtropical water (Menezes et al., 2013). Moreover, recent studies noted a meridional salinity dipole mode in the Indian Ocean with the southeast pole located in the SEIO (Zhang et al., 2016, 2018). This mode is correlated with ENSO and Indian Ocean Dipole (IOD) on interannual timescale and also associated with decadal modulation of the Indo-Pacific Walker circulation, which means that it would serve as a good indicator of climate variability (Zhang et al., 2018). The significance of salinity in the SIO implies that it is meaningful to better understand its variability and impacts on multiple spatiotemporal scales.

This study aims to further illustrate the salinity variability in the SIO and quantify its influence on the regional sea level changes, with an emphasis on the decadal characteristics in the SEIO. While it has been recognized that the decadal freshening in the upper SEIO conspicuously contributes to the local sea level rise during the GSWS, there is still a lack of quantitative estimation for the cause and impact of this interesting decadal freshening phenomenon. Furthermore, with the end of GSWS, the Indo-Pacific sea level has shifted to a decline phase since the early 2010s. The possible impact of SIO salinity on this decadal phase change in sea level deserves further clarification as well. In this study, we utilize the observational data and the results from a model of the Consortium for Estimating the Circulation and climate of the Ocean (ECCO) to investigate the respective roles of ocean dynamics and atmospheric forcing in the upper-ocean salinity balance and subsequent sea level change in the SIO. The paper is organized as below. The data and methods are described in Section 2. Based on the observational data and the global ocean model simulations, Section 3 presents the decadal sea level variability in the SIO and highlights the contributions from salinity changes. Then the salinity budget analysis is applied to further clarify the causes of salinity changes. Section 4 provides a summary and discusses the possible future work motivated by the present study.

2 Data and methods

2.1 *Observational data*

In this study, we adopt a gridded dataset on sea level anomalies from multi-satellite altimeters, which was previously provided by Archiving, Validation and Interpretation of Satellite Oceanographic data (AVISO), is now processed and distributed by the Copernicus Marine Environment Monitoring Service (CEMES). The dataset is available on a 0.25°×0.25° spatial resolution and interpolated to daily with an optimal computation time window (6 weeks before and after the date). As we study the variability on seasonal and longer timescales, the original daily sea level data are temporally averaged to be a monthly dataset.

Argo, commonly known as "ARGO Global Ocean Observation Network", is a component of the Global Ocean Observing System. The Argo-based temperature and salinity products used in this paper are monthly average gridding data from 2004 to 2017 provided by the Scripps Institution of Oceanography (Roemmich and Gilson, 2009). The dataset has a horizontal grid spacing of 1°×1° and 58 vertical isobaric layers. The vertical resolutions vary gradually from 10 m in the upper 170 m to 100 m in the depth of ~2 000 m.

2.2 *ECCO reanalysis product*

ECCO is a global ocean assimilation product obtained by combining the Massachusetts Institute of Technology General Circulation Model (MITgcm; Marshall et al., 1997) with most available ocean data in a physically and statistically consistent manner (Forget et al., 2015). In this study, we use monthly output of the newly-released ECCO version 4 Release 4 (ECCOv4r4), which covers the period from 1992 to 2017 [①]. It has a zonal resolution of 1° and the meridional resolutions varying from ~(1/3°)

[①] Fukumori I, Wang Ou, Fenty I, et al. 2019. ECCO Version 4 Release 4 Notes. https://ecco.jpl.nasa.gov/drive/files/Version4/Release4/doc/v4r4_synopsis.pdf

near the equator to ~1° in the middle and high latitudes. There are 50 vertical layers with varying resolutions from 10 m in the upper ocean to 400 m at the maximum depth of 5 906 m. ECCOv4r4 is constrained by a variety of ocean observations, including satellite altimetry, sea surface temperature/salinity, *in situ* hydrography, ocean mass from satellite gravity and sea-ice concentration ①. Through the adjoint method, its initial conditions, surface atmospheric state and internal parameters are iteratively optimized to fit multiple sources of observations within expected uncertainties. One significant advantage of ECCOv4r4 product is that it retains physical consistency through the conservation laws encoded in the model. This feature enables the closure of salinity budgets with negligible budget residuals (Forget et al., 2015). The mixing effect consists of turbulent diffusion, Gent-McWilliams density mixing (Gent and McWilliams, 1990) and K-profile parameterization vertical mixing (Large et al., 1994), which are beneficial to quantitatively evaluate the impact of these subgrid processes.

2.3 *Salinity budget*

The salinity budget is evaluated by the method similar to some previous studies (Gao et al., 2014; Wilson and Riser, 2016; Wu et al., 2019), which reads as:

$$\frac{\partial [S]}{\partial t} = \frac{(E-P)\cdot[S]}{h} - [\nabla_H \cdot (uS, vS)]_h + [\text{mixing}]_H - [\nabla_Z (wS)] + [\text{mixing}]_Z, \quad (1)$$

where the square bracket means the depth average within the upper layer h. Given that the decadal salinity change mainly occurs in the upper ocean (figure not shown), here h is defined as the upper 300 m, the same as the setting in Llove and Lee (2015). The u, v and w are the zonal, meridional and vertical velocities, respectively. Horizontal and vertical components of a variable are denoted by subscript H and Z, respectively. The $\nabla_H = \left(\frac{\partial}{\partial x}, \frac{\partial}{\partial y}\right)$ and $\nabla_Z = \frac{\partial}{\partial z}$ denote the horizontal gradient operator and vertical gradient operator. The terms on right side of Eq. (1) represent, from left to right, surface freshwater forcing (SFF for short), horizontal salt advection, horizontal mixing component, vertical salt entrainment and vertical mixing component, respectively. The sum of last four terms is referred to as the effect of ocean dynamics (ODY for short). Each variable in Eq. (1) could be separated into two parts: the interannual-to-decadal variability and the climatological seasonal cycle (e.g., $S = S' + \bar{S}$). Then the horizontal salinity advection term could be decomposed into the four terms as follows:

$$-[\nabla_H \cdot (uS, vS)]_h = -\left[\left(\bar{u}\frac{\partial \bar{S}}{\partial x} + \bar{v}\frac{\partial \bar{S}}{\partial y}\right) + \left(\bar{u}\frac{\partial S'}{\partial x} + \bar{v}\frac{\partial S'}{\partial y}\right) + \left(u'\frac{\partial \bar{S}}{\partial x} + v'\frac{\partial \bar{S}}{\partial y}\right) + \left(u'\frac{\partial S'}{\partial x} + v'\frac{\partial S'}{\partial y}\right)\right]. \quad (2)$$

The first term is the mean background advection only containing seasonal signals. The second and third terms indicate the low-frequency salinity variability induced by the anomalous salinity gradient $\left(\bar{u}\frac{\partial S'}{\partial x} + \bar{v}\frac{\partial S'}{\partial y}\right)$ and by the anomalous ocean current $\left(u'\frac{\partial \bar{S}}{\partial x} + v'\frac{\partial \bar{S}}{\partial y}\right)$, respectively. The fourth term represents the higher-order nonlinear effect, which is usually much smaller than the other terms.

3 Results

3.1 *Sea level changes*

As noted in several previous studies, sea level in Indo-Pacific shows decadal rise from 2005 to 2012 and subsequent decline since ~2013 (Llove and Lee, 2015; Meng et al., 2019). Generally following the previous results, Figs 1a and b show the regional patterns of altimetric sea level trends over the periods of 2005–2013 and 2013–2017. It could be clearly seen that sea level trends in most regions have opposite signs between these two periods, demonstrating the significant decadal phase reversal. In Fig. 1a, the most significant sea level rise occurs in the tropical the Northwest Pacific (5°–10°N, 120°–140°E) and the SEIO (8.5 °–29.5°S, 80.5°–113.5°E), with regional mean values of 17.68 mm/a and 10.26 mm/a, respectively. In the period of 2013–2017, the sea level obviously declines in the above two regions (Fig. 1b). Figures 1c and d show the trends of upper 300 m ocean steric sea level in the periods of 2005–2013 and 2013–2017, respectively. The trend patterns of steric height are quite similar to the total sea level trends from altimeter observations. But the trend magnitudes in steric height are obviously less. During 2005–2013, the steric height in the Northwest Pacific rises at a mean rate of 9.20 mm/a, which explains only 52% of the total trend, indicating the substantial contributions from deeper ocean density changes or mass-induced component. By contrast, in the SEIO, the rise trend of steric sea level is 6.77 mm/a during 2005–2013, accounting for 66% of the total trend, reflecting the larger impacts of upper ocean density changes on the decadal trends of regional sea level. To further quantify the depth dependence of the steric height in the SEIO, we also calculate the surface steric height relative to the depth of 2 000 m. Compared with the linear trends of steric height in Figs 1c and d, the decadal trends of steric height referenced to 2 000 m are only ~10% larger in the SEIO (figure not shown). It means that in the SEIO, the intermediate-deep layer waters exert little impact on the total sea level trends.

In order to evaluate the respective effects of temperature and salinity on the steric sea level variability, we estimate the thermosteric and halosteric height by replacing in the equation of state for seawater the time-varying $S(x, y, z, t)$ and $T(x, y, z, t)$ with the time-averaged $\bar{S}(x, y, z)$ and $\bar{T}(x, y, z)$ during 2004–2017. In both periods, the thermosteric sea level is the primary contribution to the trends of streic sea level in many regions (Figs 1e and f), while the trends of halosteric sea level are generally smaller and tend to compensate the trends of thermosteric component in western Pacific (Figs 1g and h). Only in the SEIO, the thermosteric and halosteric sea level components show consistent decadal trends with comparable magnitudes. During 2005–2013, the rise trends induced by the thermosteric and halosteric effects are 3.79 mm/a and 2.92 mm/a, respectively, in the SEIO (Figs 1e and g). After the decadal phase reversal, both components shift to the decline trends with the rates of –5.10 mm/a for thermosteric sea level and –2.98 mm/a for halosteric one, respectively (Figs 1f and h). The above results demonstrate that the halosteric effect not only has a large contribution to the sea level rise during 2005–2013, which has been noted in Llovel and Lee (2015), but also persistently contributes to the sea level decline after the decadal phase change since 2013.

To further depict the sea level variations on multiple timescale, Fig. 2a shows the time series of total sea level in the SEIO and its steric, thermosteric and halosteric components. Consid-

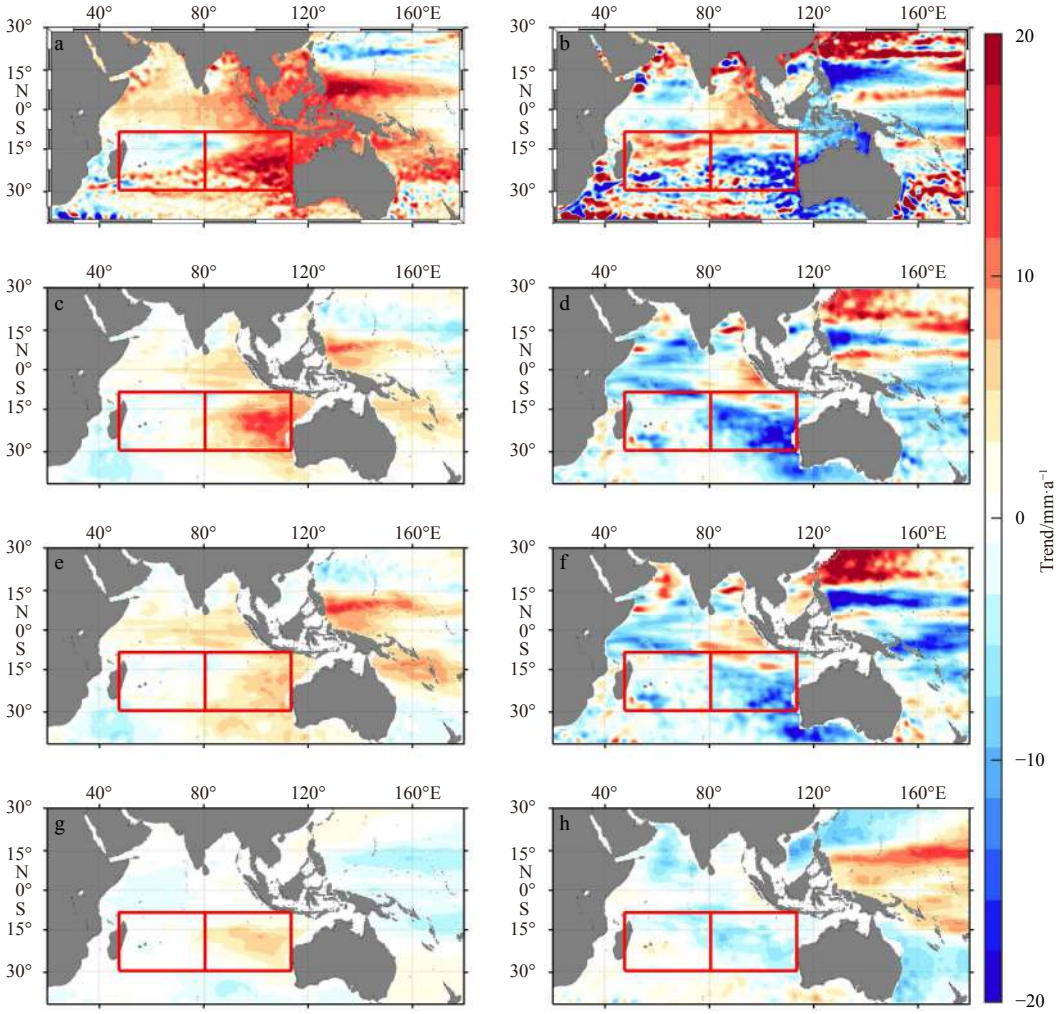

Fig. 1. Linear trends of sea level in 2005–2013 derived from satellite altimeter data (a), the steric sea level based on Argo data (c), the thermosteric sea level based on Argo data (e), the halosteric sea level based on Argo data (g). Figures b, d, f, h are the same as a, c, e, g, respectively, but for the period of 2013–2017. The reference level used to compute steric sea level in Figs c–h is 300 m.

ering that significant decadal trends in sea level mainly occur in the SEIO, we also select the southwest Indian Ocean (SWIO, 8.5°–29.5°S, 47.5°–80.5°E) as a counterpart to highlight the difference in sea level variability between the eastern and western basins of SIO. The sea level time series in both regions display low-frequency fluctuations embedded with remarkable seasonal cycles (Figs 2a and b). Seasonal signals are also remarkable in the time series of steric height and its thermosteric component, but are much weaker in the time series of halosteric component, suggesting that thermosteric effects largely explain the seasonal variations of both steric and total sea level. After removal of the seasonal signals, the interannual-to-decadal time series in the SEIO show obvious sea level rise until 2013 and subsequent sea level decline afterwards (Fig. 2c), consistent with the results in Fig. 1. Nevertheless, the low-frequency sea level variability in the SWIO is dominated by the interannual signals and does not exhibit evident decadal trends (Fig. 2d). The interannual signals of steric height are largely controlled by the thermosteric effect. The halosteric effect only slightly enhances or compensates the contributions from thermosteric component. Meanwhile, because we only consider the variations in the upper 300 m, the low-frequency steric signals in both SEIO and SWIO resemble the altimeter observations but display weaker amplitudes. The difference between total and steric heights are more pronounced in the SWIO probably due to the thermocline deepening in the center of subtropical gyre to the east of Madagasscar Island. The depth dependence of the SIO subtropical gyre variability is another interesting topic. But it is beyond the scope of the present study and will not be further discussed here.

3.2 *ECCO model validations*

Given the importance of halosteric effect to the decadal sea level variability in the SEIO, the model outputs from ECCOv4r4 are utilized to further elucidate the causes of decadal salinity changes through the budget analysis as introduced in Section 2.3. Before investigating the physical processes related to the salinity changes, we first validate the performance of ECCOv4r4 model in the SIO by comparing the simulated interannual-to-decadal variations in sea level and upper 300 m salinity with the altimeter and Argo observations. As shown in Figs 3a and b, the observed and simulated sea level signals display very similar low-frequency variability, with a correlation coefficient of 0.98 for both the SEIO and the SWIO (Figs 3a and b). The model results could simulate both the observed multi-decadal trend from 1993 to 2013 and the

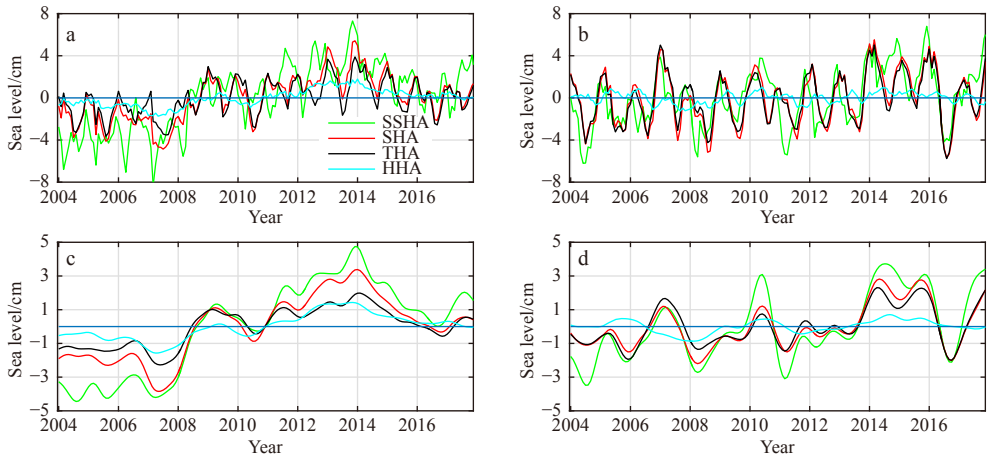

Fig. 2. The time series of sea surface height anomaly (SSHA), steric height anomaly (SHA), thermosteric height anomaly (THA) and halosteric height anomaly (HHA) during 2004–2017 in the SEIO (a), and the SWIO (b). Figures c, d are similar to a, b but for low-frequency variations (with periods>13 month). The low-frequency signals are derived by subtracting the monthly climatological mean from the original data and then applying a 13-month Hanning filter to suppress the sub-seasonal signals. Steric height and its thermosteric and halosteric components are relative to the depth of 300 m.

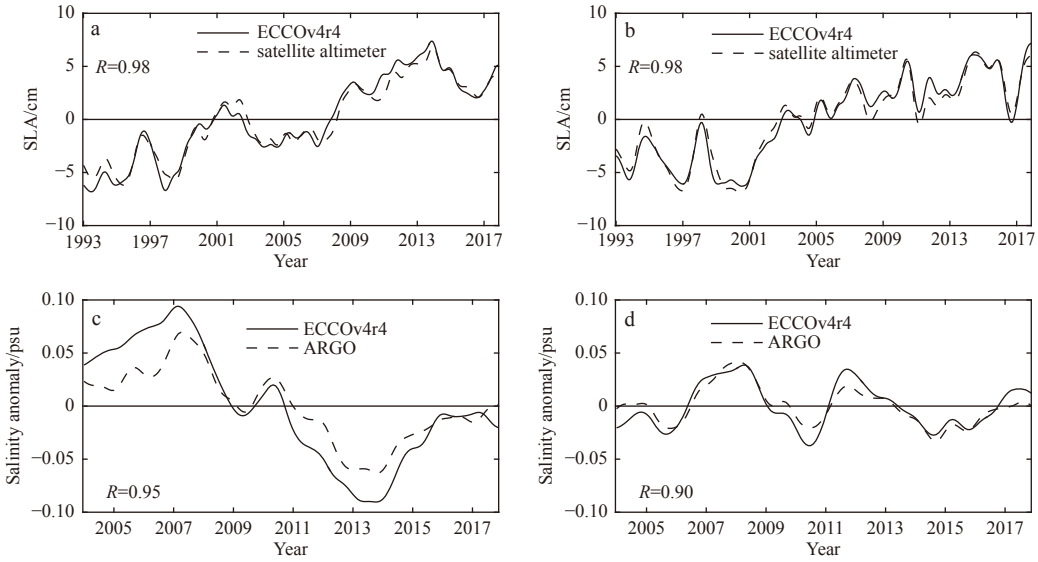

Fig. 3. Interannual-to-decadal variability of sea level anomalies during 1993–2017 derived from altimeter observations (dashed lines) and ECCOv4r4 (solid lines) in the SEIO (a), and the SWIO (b). Interannual-to-decadal variability of upper 300 m mean salinity during 2004–2017 from Argo observations (dashed lines) and ECCOv4r4 (solid lines) in the SEIO (c), and the SWIO (d). The low-pass filter applied here is the same as Fig. 2.

embedded interannual-to-decadal fluctuations. Meanwhile, ECCOv4r4 also well captures the observed upper-ocean salinity variations in the SIO. In the SEIO, both observations and ECCO simulations show remarkable freshening of surface water during 2005–2013 and the salinity rebound from 2013 to 2017 (Fig. 3c). The model-data correlation between observations and simulations reaches 0.95 in the period of 2004–2017. Similarly, in the SWIO, the simulated salinity variability also well resembles the observations with a correlation coefficient of 0.93. But the upper-ocean salinity in the SWIO is dominated by relatively higher frequency interannual oscillations and does not show obvious decadal phase reversal before and after 2013. The observed seasonal variations of salinity are also reasonably reproduced in the ECCO model. Both observations and simulations in the SIO show the characteristics of lower salinity in austral fall and higher salinity in austral spring (figures not shown). Therefore, the model-observation agreement makes it practicable to use the ECCO product to study the underlying processes associated with the upper salinity changes in the SIO.

3.3 *Causes of decadal trends of upper-ocean salinity in the SIO*

According to the salinity budget method introduced in Section 2.3, the terms in the salinity balance from ECCOv4r4 are used in this section to diagnose the upper ocean salinity budget in the SIO. In both the SEIO and SWIO, the salinity tendencies are almost the same as the sum of all forcing terms (Figs 4a and b), suggesting that the salinity balance resulting from ECCOv4r4 is closed. The salinity tendency term in the SEIO tends to be negat-

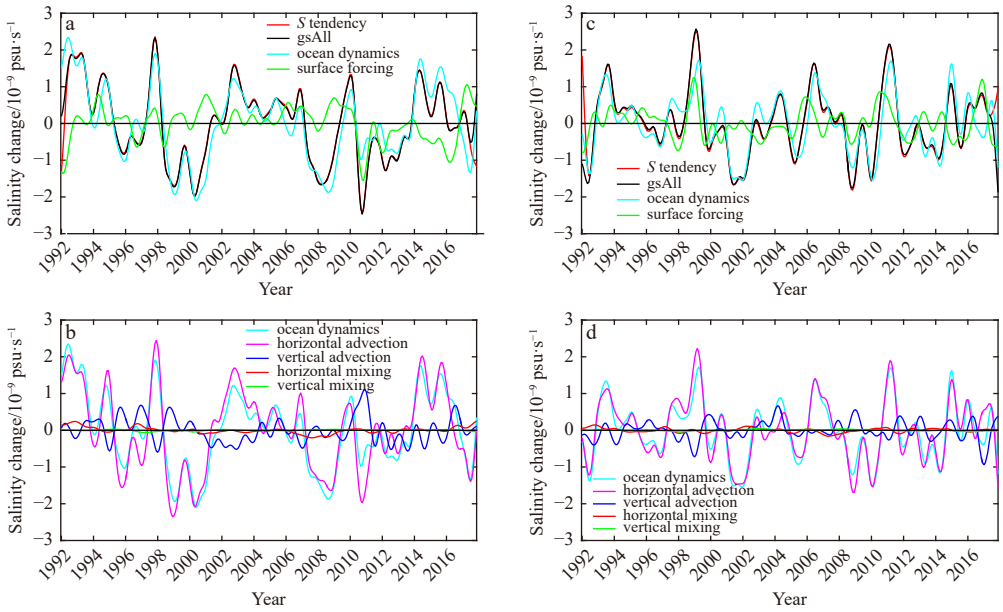

Fig. 4. Interannual-to-decadal variations of ECCOv4r4 salinity balance in the upper 300 m. a. Salinity tendency (red), sum of all forcing terms (black), ODY (cyan) and SFF (green) terms in the SEIO; and b. ODY term (cyan) in the SEIO and its four components in Eq. (1). Figures c and d are similar to Figs a and b, respectively, but for the results in the SWIO. The low-pass filter applied here is the same as Fig. 2.

ive during 2005–2013 with some positive exceptions during the El Niño events, such as the 2009/2010. It reflects the decadal freshening trend in SEIO modulated by interannual signals shown in Fig. 3c. The tendency term shifts to positive phase during 2013–2017, corresponding to the increase of upper-ocean salinity. Consistent with the salinity changes in Fig. 3d, its tendency term in the SWIO mainly exhibits interannual fluctuations as well (Fig. 4b). In most cases, the ODY terms are larger in magnitude than the SFF terms and thus account for the major part of the salinity tendencies in both regions. The correlation coefficients between salinity tendencies and ODY terms are 0.86 and 0.84 for the SEIO and SWIO, respectively. Compared with the varying amplitude of tendency term, the amplitude of ODY is very close in the SEIO, but slightly weaker in the SWIO, indicating that the ocean process plays a more important role in the salinity variability in the SEIO.

The relative importance of the four specific terms of ODY, including horizontal advection, vertical advection, horizontal mixing and vertical mixing, are further compared in Figs 4c–d . It is obvious that, in both SEIO and SWIO, the horizontal advection is the main component of the ODY. The effect of vertical advection is obviously smaller in magnitude and usually compensates the effect of horizontal advection. Compared with the advection effects, the contributions from horizontal and vertical mixing are both negligible.

Figure 5 further shows the spatial distributions of anomalous salinity tendency, SFF and ODY in 2005–2013. During this period, the upper-ocean salinity decreases in the South China Sea, the Indonesian seas and the SEIO, but increases in the tropical western Pacific (Fig. 5a). The salinity decrease in the SEIO mainly occurs over the strong mean salinity front between the tropical low-salinity water and the subtropical high-salinity water. The SFF exerts strong negative effect around the Indonesian Archipelago (Fig. 5b). Consistent with the SFF, the sea surface wind anomalies in Fig. 5b show convergence over this region, indicative of

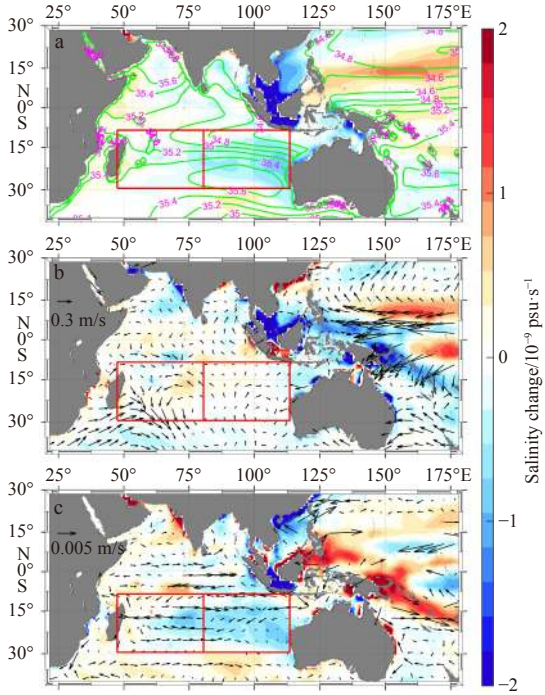

Fig. 5. The anomalous salinity budget terms in the upper 300 m during 2005–2013. a. Salt tendency (shading) and mean salinity (green contours), b. SFF term (shading) and surface wind anomalies (vectors), and c. ODY term (shading) and anomalous upper-ocean velocities (vectors). To highlight the anomalies in the SIO, the wind speed larger than 1 m/s and ocean current larger than 0.01 m/s are removed from Figs b and c, respectively.

anomalous precipitation induced by enhanced atmospheric deep convection. The ODY shows a negative pattern similar to salinity tendency in the SEIO and strong positive values around

the Indonesian Archipelago (Fig. 5c). The anomalous ocean current indicates an enhanced ITF, which transports the anomalous signals of SFF westward and thus leads to the salinity decrease (increase) in the Indian Ocean (Indonesian seas) and a weakened South Equatorial Current (SEC). It is noteworthy that the anomalous SEC and ITF converge at around 100°E and 15°S, forming a southward flow anomaly in the subtropical SEIO. Previous studies have noted this anomalous southward flow during the GSWS and pointed out that it played a key role in conveying the ocean heat from the tropical Indian Ocean to the Southern Ocean (Li et al., 2017; Liao et al., 2019).

The spatial distributions of anomalous salinity budget terms in 2013–2017, as shown in Fig. 6, are generally opposite to those in 2005–2013. The upper-ocean salinity decreases in the tropical western Pacific and increases in the South China Sea, the SEIO and to north of Australia (Fig. 6a). Associated with the relatively weak wind anomalies, the SFF term shows a complex and spotty pattern over the equatorial Pacific and Indonesian seas, which means that there is no spatially uniformed anomalous SFF in this period (Fig. 6b). The similar spatial patterns of salinity tendency and ODY (Figs 6a and c) confirm that in most of the Indo-Pacific region, ODY plays a leading role in the decadal salinity trends during 2013–2017. Comparing the Figs 5c and 6c, we could see that in the SIO, the anomalous flow pattern in 2013–2017 is generally opposite to that in 2005–2013. The northeastward flow anomaly in the Indonesian Seas indicates the weakening of ITF (Fig. 6c). The enhanced SEC and weakened ITF induce the upper-ocean divergence around 100°E and 15°S, and subsequently result in an anomalous northward flow in the subtropical SEIO (Fig. 6c). The positive ODY and northward flow anomalies in the

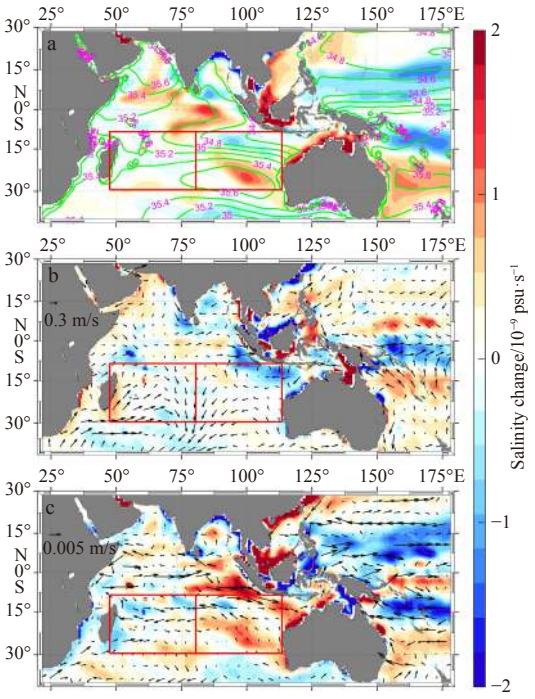

Fig. 6. The anomalous salinity budget terms in the upper 300 m during 2013–2017. a. Salt tendency (shading) and mean salinity (green contours), b. SFF term (shading) and surface wind anomalies (vectors), and c. ODY term (shading) and anomalous upper-ocean velocities (vectors). The wind speed larger than 1 m/s and ocean current larger than 0.01 m/s are removed from Figs b and c, respectively.

SEIO suggest that weaker horizontal advection may be an important factor for the salinity increase in this period.

In order to further clarify the respective effects of salinity anomalies and velocity anomalies on the upper-ocean salinity tendency, the horizontal advection term is decomposed into six components following the Eq. (2). Figure 7 shows the spatial distribution of each component of horizontal advection term during 2005–2013. The effect of $-v'\frac{\partial \bar{S}}{\partial y}$ term (Fig. 7b) is definitely the main cause of the freshening in the SEIO. It results from the joint effects of two factors: one is the strong meridional mean salinity gradient as shown in Fig. 5a, another is the anomalous southward current in the SEIO, which originates at the convergence zone between the weakened SEC and the enhanced ITF (Li et al., 2017; Liao et al., 2019). By contrast, due to the weaker zonal salinity gradient, zonal advection associated with $-u'\frac{\partial \bar{S}}{\partial x}$ does not show significant impacts on the freshening in the SEIO (Fig. 7a). The intense evaporation leads to the zonally extended high salinity band in the subtropical SIO (Toole and Warren, 1993; Pokhrel et al., 2012). Meanwhile, the local precipitation and freshwater transport by ITF form the low salinity zone in the tropical SIO (Qu and Meyers, 2005). The present study shows that the mean salinity front between the above two water masses plays an essential role in the decadal salinity change in the SEIO. The $\bar{u}\frac{\partial S'}{\partial x}$ and $\bar{v}\frac{\partial S'}{\partial y}$ appear to be important components of horizontal advection term in the equatorial Pacific and northern Indian Ocean (Fig. 7c-d). But their influences are minor in the SEIO. In addition, the higher-order nonlinear terms $\left(-u'\frac{\partial S'}{\partial x} \text{ and } -v'\frac{\partial S'}{\partial y}\right)$ also have considerable influences in tropical and northern Indian Ocean, but have little contribution to the SEIO salinity changes (Fig. 7e-f). During 2013–2017, the $-v'\frac{\partial \bar{S}}{\partial y}$ also dominates the salinity increase in the SEIO (figure not shown). As shown in Fig. 6c, due to the enhanced SEC and weakened ITF, the upper-ocean divergence around 100°E and 15°S lead to a northward flow anomaly in the SEIO, which subsequently results in a strong positive $-v'\frac{\partial \bar{S}}{\partial y}$. Therefore, we could conclude that it is the decadal variability of meridional current and the mean spatial pattern of salinity front in the SIO that governs the decadal salinity variations in the SEIO.

4 Discussion and summary

Using the Argo data, satellite observations and the ECCOv4r4 ocean reanalysis, this study investigates the decadal sea level and salinity changes in the SIO during 2005–2017. Particular attentions are paid to the potential role of salinity effect in the decadal sea level change over the SEIO. The results show that the sea level change on the seasonal scale is primarily thermosteric in nature and is not essentially influenced by the variations of salinity in the whole SIO. Nevertheless, the interannual-to-decadal sea level variability in the SEIO is significantly modulated by the halosteric effect associated with the upper-ocean salinity variations. Especially on decadal timescale, due to the wave transmissions along the Indo-Pacific waveguides, sea level in both the western Pacific and the SEIO experiences a coherent phase reversal from the rise phase during 2005–2013 to the decline phase during 2013–2017. However, the relative importance of temperature and salinity effects are distinct between the western Pacific and the SEIO. In the SEIO, the thermosteric and halosteric components

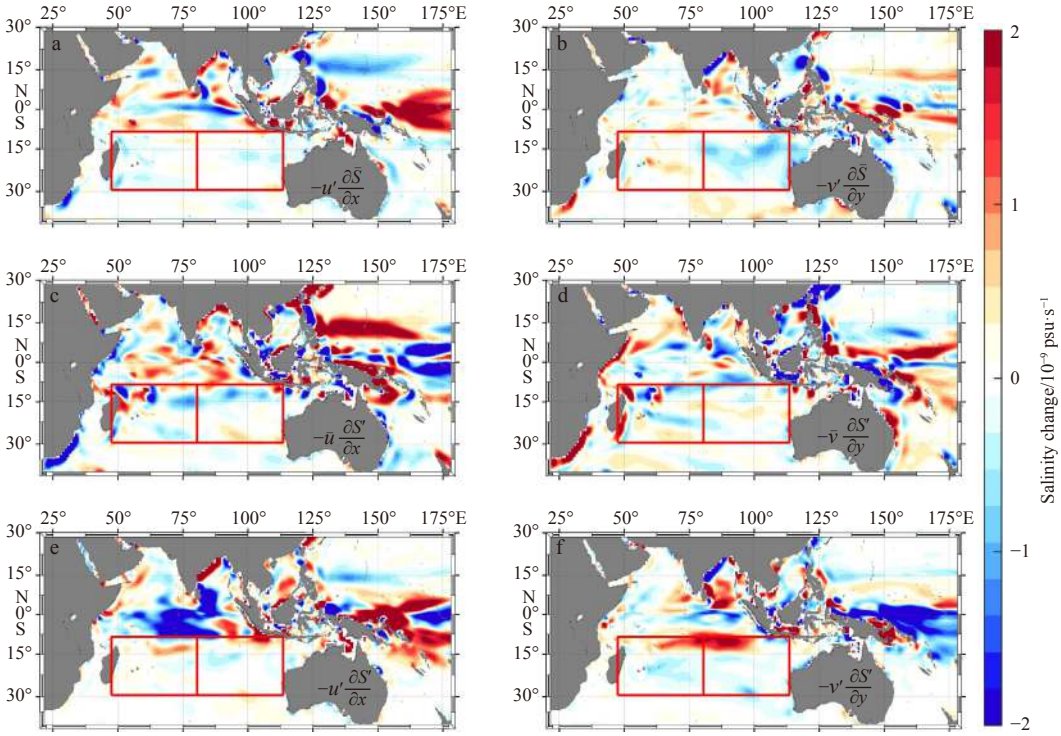

Fig. 7. Decomposition of the horizontal advection term in 2005–2013. a. The zonal advection associated with anomalous currents and mean salinity gradient, c. the zonal advection associated with mean currents and anomalous salinity gradient, e. the zonal advection associated with anomalous currents and anomalous salinity gradient, and b, d and f is similar to a, c and e, respectively, but for the meridional advections.

have comparable positive contributions to the decadal variability of sea level. By contrast, the western Pacific sea level is dominated by thermosteric component and the halosteric one tends to have negative contributions. In addition, in the SWIO and northern Indian Ocean, the decadal sea level variations are usually little affected by salinity changes.

The salinity budget analyses based on the ECCO reanalysis are used to further explore the causes of upper-ocean salinity changes in the SEIO. The results indicate that the oceanic horizontal advection in the ODY is the key contributor to the decadal variability of upper-ocean salinity around the SEIO. Further decomposition on the horizontal advection term suggests that the decadal freshwater transport is largely caused by the $-v'\frac{\partial \bar{S}}{\partial y}$ term, that is, the anomalous meridional currents in the SEIO on the background of a strong salinity front between the tropical freshwater and subtropical saltier water. However, the others components of ODY, including vertical advection, horizontal and vertical mixing, do not have significant contribution to the decadal phase changes of salinity and sea level from 2005–2013 to 2013–2017.

To evaluate the possible effect of eddy-induced salinity transport, we further compared the large-scale salinity advection due to the resolved velocity and the eddy-induced salinity advection associated with the parameterized bolus velocity in the period of 2005–2013. As shown in Fig. 8, the estimation of ECCOv4r4 suggests that the freshwater transport induced by bolus velocity is much weaker than the effects of resolved velocity, meaning that the effects from the eddy-induced transport is smaller than the contributions of the resolved flow. However, due to the relatively coarse model resolution, the eddy-induced transport may probably not be well reproduced in the ECCOv4r4 ocean state estimate. In fact, the eddy activities in the SEIO are strong and exhibit significant variability on seasonal and interannual timescales (e.g., Zheng et al., 2018). The eddy-induced transport deserves more accurate evaluations in the framework of eddy-resolving assimilation system. Overall, the above results prove the exceptionally crucial role of salinity in the SEIO. In particular, the linkages among circulation, salinity and sea level change have been further clarified. It will be important for future studies to further clarify their interactions under the circumstance of the climate

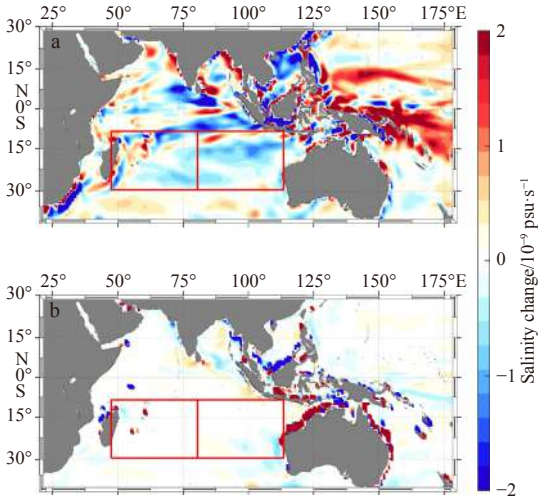

Fig. 8. The horizontal salinity advection in 2005–2013 induced by the resolved velocity (a) and the bolus velocity (b).

variability and climate change.

Acknowledegements

The altimeter satellite gridded products were produced by Copernicus Marine Environment Monitoring Service (CEMES). (http://marine.copernicus.eu/services-portfolio/access-to-products). The Argo data were collected and made freely available by the International Argo Program at http://www.argo.ucsd.edu. The ECCO v4r4 data could be downloaded from https://ecco.jpl.nasa.gov/drive/files/Version4/Release4/.

References

Cai Wenju, Meyers G, Shi Ge. 2005. Transmission of ENSO signal to the Indian Ocean. Geophysical Research Letters, 32(5): L05616

Chen Xianyao, Zhang Xuebin, Church J A, et al. 2017. The increasing rate of global mean sea-level rise during 1993–2014. Nature Climate Change, 7(7): 492–495, doi: 10.1038/nclimate3325

Cheng Xuhua, Li Lijuan, Du Yan, et al. 2013. Mass-induced sea level change in the northwestern North Pacific and its contribution to total sea level change. Geophysical Research Letters, 40(15): 3975–3980, doi: 10.1002/grl.50748

Du Yan, Zhang Yuhong, Feng Ming, et al. 2015. Decadal trends of the upper ocean salinity in the tropical Indo-Pacific since mid-1990s. Scientific Reports, 5: 16050, doi: 10.1038/srep16050

Du Yan, Zhang Yuhong, Shi Jiancheng. 2019. Relationship between sea surface salinity and ocean circulation and climate change. Science China Earth Sciences, 62(5): 771–782, doi: 10.1007/s11430-018-9276-6

Feng Ming, McPhaden M J, Lee T. 2010. Decadal variability of the Pacific subtropical cells and their influence on the southeast Indian Ocean. Geophysical Research Letters, 37(9): L09606

Forget G, Campin J M, Heimbach P, et al. 2015. ECCO version 4: an integrated framework for non-linear inverse modeling and global ocean state estimation. Geoscientific Model Development, 8(10): 3071–3104, doi: 10.5194/gmd-8-3071-2015

Gao Shan, Qu Tangdong, Nie Xunwei. 2014. Mixed layer salinity budget in the tropical Pacific Ocean estimated by a global GCM. Journal of Geophysical Research: Oceans, 119(12): 8255–8270, doi: 10.1002/2014JC010336

Gent P R, McWilliams J C. 1990. Isopycnal mixing in ocean circulation models. Journal of Physical Oceanography, 20(1): 150–155, doi: 10.1175/1520-0485(1990)020<0150:IMIOCM>2.0.CO;2

Gill A E, Niller P P. 1973. The theory of the seasonal variability in the ocean. Deep Sea Research and Oceanographic Abstracts, 20(2): 141–177, doi: 10.1016/0011-7471(73)90049-1

Hamlington B D, Cheon S H, Thompson P R, et al. 2016. An ongoing shift in Pacific Ocean sea level. Journal of Geophysical Research: Oceans, 121(7): 5084–5097, doi: 10.1002/2016JC011815

Han Weiqing, Stammer D, Meehl G A, et al. 2018. Multi-decadal trend and decadal variability of the regional sea level over the Indian Ocean since the 1960s: Roles of climate modes and external forcing. Climate, 6(2): 51, doi: 10.3390/cli6020051

Hu Shijian, Sprintall J. 2017. Observed strengthening of interbasin exchange via the Indonesian seas due to rainfall intensification. Geophysical Research Letters, 44(3): 1448–1456, doi: 10.1002/2016GL072494

Jyoti J, Swapna P, Krishnan R, et al. 2019. Pacific modulation of accelerated south Indian Ocean sea level rise during the early 21st Century. Climate Dynamics, 53(7–8): 4413–4432, doi: 10.1007/s00382-019-04795-0

Köhl A. 2014. Detecting processes contributing to interannual halosteric and thermosteric sea level variability. Journal of Climate, 27(6): 2417–2426, doi: 10.1175/JCLI-D-13-00412.1

Large W G, McWilliams J C, Doney S C. 1994. Oceanic vertical mixing: A review and a model with a nonlocal boundary layer parameterization. Reviews of Geophysics, 32(4): 363–403, doi: 10.1029/94RG01872

Li Yuanlong, Han Weiqing. 2015. Decadal sea level variations in the Indian Ocean investigated with HYCOM: Roles of climate modes, ocean internal variability, and stochastic wind forcing. Journal of Climate, 28(23): 9143–9165, doi: 10.1175/JCLI-D-15-0252.1

Li Yuanlong, Han Weiqing, Zhang Lei. 2017. Enhanced decadal warming of the southeast Indian Ocean during the recent global surface warming slowdown. Geophysical Research Letters, 44(19): 9876–9884, doi: 10.1002/2017GL075050

Liao Enhui, Yan Xiaohai, Jiang Yuwu, et al. 2019. New findings on the route of heat transport between the Indo-Pacific and Southern Ocean. Climate Dynamics, 52(9–10): 5145–5151, doi: 10.1007/s00382-018-4436-4

Llovel W, Lee T. 2015. Importance and origin of halosteric contribution to sea level change in the southeast Indian Ocean during 2005-2013. Geophysical Research Letters, 42(4): 1148–1157, doi: 10.1002/2014GL062611

Marshall J, Adcroft A, Hill C, et al. 1997. A finite-volume, incompressible Navier Stokes model for studies of the ocean on parallel computers. Journal of Geophysical Research: Oceans, 102(C3): 5753–5766, doi: 10.1029/96JC02775

Menezes V V, Phillips H E, Schiller A, et al. 2013. Salinity dominance on the Indian Ocean Eastern Gyral current. Geophysical Research Letters, 40(21): 5716–5721, doi: 10.1002/2013GL057887

Meng Lingsheng, Zhuang Wei, Zhang Weiwei, et al. 2019. Decadal sea level variability in the Pacific Ocean: Origins and climate mode contributions. Journal of Atmospheric and Oceanic Technology, 36(4): 689–698, doi: 10.1175/JTECH-D-18-0159.1

Merrifield M A, Thompson P R, Lander M. 2012. Multidecadal sea level anomalies and trends in the western tropical Pacific. Geophysical Research Letters, 39: L13602

Nidheesh A G, Lengaigne M, Vialard J, et al. 2013. Decadal and long-term sea level variability in the tropical Indo-Pacific Ocean. Climate Dynamics, 41(2): 381–402, doi: 10.1007/s00382-012-1463-4

Pokhrel S, Rahaman H, Parekh A, et al. 2012. Evaporation-precipitation variability over Indian Ocean and its assessment in NCEP Climate Forecast System (CFSv2). Climate Dynamics, 39(9–10): 2585–2608, doi: 10.1007/s00382-012-1542-6

Qiu Bo, Chen Shuming. 2012. Multidecadal sea level and gyre circulation variability in the northwestern tropical Pacific Ocean. Journal of Physical Oceanography, 42(1): 193–206, doi: 10.1175/JPO-D-11-061.1

Qu Tangdong, Meyers G. 2005. Seasonal characteristics of circulation in the southeastern tropical Indian Ocean. Journal of Physical Oceanography, 35(2): 255–267, doi: 10.1175/JPO-2682.1

Roemmich D, Gilson J. 2009. The 2004–2008 mean and annual cycle of temperature, salinity, and steric height in the global ocean from the Argo Program. Progress in Oceanography, 82(2): 81–100, doi: 10.1016/j.pocean.2009.03.004

Roemmich D, Johnson G, Riser S, et al. 2009. The Argo Program: Observing the global ocean with profiling floats. Oceanography, 22(2): 34–43, doi: 10.5670/oceanog.2009.36

Schott F A, Xie Shangping, McCreary J P Jr. 2009. Indian Ocean circulation and climate variability. Reviews of Geophysics, 47(1): RG1002

Stammer D, Cazenave A, Ponte R M, et al. 2013. Causes for contemporary regional sea level changes. Annual Review of Marine Science, 5(1): 21–46, doi: 10.1146/annurev-marine-121211-172406

Toole J M, Warren B A. 1993. A hydrographic section across the subtropical South Indian Ocean. Deep Sea Research Part I: Oceanographic Research Papers, 40(10): 1973–2019, doi: 10.1016/0967-0637(93)90042-2

Vinogradov S V, Ponte R M, Heimbach P, et al. 2008. The mean seasonal cycle in sea level estimated from a data-constrained general circulation model. Journal of Geophysical Research: Oceans, 113(C3): C03032

Wijffels S, Meyers G. 2004. An intersection of oceanic waveguides: Variability in the Indonesian Throughflow region. Journal of Physical Oceanography, 34(5): 1232–1253, doi: 10.1175/1520-0485(2004)034<1232:AIOOWV>2.0.CO;2

Willis J K, Chambers D P, Kuo C Y, et al. 2010. Global sea level rise: Recent progress and challenges for the decade to come. Ocean-

ography, 23(4): 26–35, doi: 10.5670/oceanog.2010.03

Wilson E A, Riser S C. 2016. An assessment of the seasonal salinity budget for the upper Bay of Bengal. Journal of Physical Oceanography, 46(5): 1361–1376, doi: 10.1175/JPO-D-15-0147.1

Wu Quran, Zhang Xuebin, Church J A, et al. 2017. Variability and change of sea level and its components in the Indo-Pacific region during the altimetry era. Journal of Geophysical Research: Oceans, 122(3): 1862–1881, doi: 10.1002/2016JC012345

Wu Quran, Zhang Xuebin, Church J A, et al. 2019. ENSO-related global ocean heat content variations. Journal of Climate, 32(1): 45–68, doi: 10.1175/JCLI-D-17-0861.1

Zhang Yuhong, Du Yan, Feng Ming. 2018. Multiple time scale variability of the sea surface salinity dipole mode in the tropical Indian Ocean. Journal of Climate, 31(1): 283–296, doi: 10.1175/JCLI-D-17-0271.1

Zhang Yuhong, Du Yan, Qu Tangdang. 2016. A sea surface salinity dipole mode in the tropical Indian Ocean. Climate Dynamics, 47(7–8): 2573–2585, doi: 10.1007/s00382-016-2984-z

Zhang Linlin, Qu Tangdong. 2015. Low-frequency variability of the South Pacific Subtropical Gyre as seen from satellite altimetry and Argo. Journal of Physical Oceanography, 45(12): 3083–3098, doi: 10.1175/JPO-D-15-0026.1

Zheng Shaojun, Feng Ming, Du Yan, et al. 2018. Interannual variability of eddy kinetic energy in the subtropical southeast Indian Ocean associated with the El Niño-Southern oscillation. Journal of Geophysical Research: Oceans, 123(2): 1048–1061, doi: 10.1002/2017JC013562